



HAL
open science

Optimizing Process Parameters of Direct Ink Writing for Dimensional Accuracy of Printed Layers

Yongqiang Tu, Javier Arrieta-Escobar, Alaa Hassan, Uzair Khaleeq Uz
Zaman, Ali Siadat, Gongliu Yang

► **To cite this version:**

Yongqiang Tu, Javier Arrieta-Escobar, Alaa Hassan, Uzair Khaleeq Uz Zaman, Ali Siadat, et al..
Optimizing Process Parameters of Direct Ink Writing for Dimensional Accuracy of Printed Layers.
3D Printing and Additive Manufacturing, 2021, 10.1089/3dp.2021.0208 . hal-03506849

HAL Id: hal-03506849

<https://hal.science/hal-03506849v1>

Submitted on 2 Jan 2022

HAL is a multi-disciplinary open access archive for the deposit and dissemination of scientific research documents, whether they are published or not. The documents may come from teaching and research institutions in France or abroad, or from public or private research centers.

L'archive ouverte pluridisciplinaire **HAL**, est destinée au dépôt et à la diffusion de documents scientifiques de niveau recherche, publiés ou non, émanant des établissements d'enseignement et de recherche français ou étrangers, des laboratoires publics ou privés.

Optimizing process parameters of direct ink writing for dimensional accuracy of printed layers

Yongqiang Tu^{a,b,*}, Javier A. Arrieta-Escobar^c, Alaa Hassan^c, Uzair Khaleeq uz Zaman^d, Ali Siadat^b, Gongliu Yang^a

(*Corresponding author: Yongqiang Tu; E-mail addresses: yongqiang.tu@ensam.eu)

^aSchool of Instrumentation and Optoelectronic Engineering, Beihang University, Beijing 100191, PR China

^bUniversité de Lorraine, Arts et Métiers ParisTech, LCFC, F-57000 Metz, France

^cUniversité de Lorraine, ERPI, F-54000 Nancy, France

^dDepartment of Mechatronics Engineering, National University of Sciences and Technology, Islamabad, Pakistan

Abstract

Direct ink writing (DIW) belongs to extrusion-based 3D printing techniques. The success of DIW process depends on well-printable ink and optimized process parameters. After ink preparation, DIW process parameters considerably affect the parts' dimensional accuracy and process parameters optimization for dimensional accuracy of printed layers is necessary for quality control of parts in DIW. In this study, DIW process parameters were identified and divided into two categories as the parameters for printing a line and the parameter from lines to a layer. Then a two-step method was proposed for optimizing process parameters. Step 1 was to optimize process parameters for printing a line. In Step 1, continuity and uniformity of extruded filaments and printed rectangular objects were observed in screening experiments to determine printability windows for each process parameter. Then, interaction effect tests were conducted and degree of freedom (DOF) for experiments was calculated followed by orthogonal array (OA) selection for Taguchi design. Next, main experiments of line printing based on Taguchi method were conducted. Signal-to-noise ratio (SNR) calculations and analysis of variance (ANOVA) were performed to find the optimal combination and evaluate the significance respectively. Step 2 was to optimize the parameter from lines to a layer. In Step 2, the average width of the printed line under optimal condition was measured firstly. Then, single-factor tests of rectangular object printing were conducted to find the optimal parameter from lines to a layer. After these two steps, confirmation results were conducted to verify the reliability of the proposed method and the method robustness on other shapes and other materials; parameter adaptability in 3D parts printing from printed layers' analyses for the proposed method and parameter adaptability in constructs fabricated as 100% infill or with porosities.

Keywords

Direct ink writing; Extrusion-based 3D printing; Process parameters optimization; Dimensional

accuracy; Taguchi method

1. Introduction

Direct ink writing (DIW), also known as extrusion-based 3D printing [1], relies on extruding ink-based materials with suitable printability through a nozzle using either mechanical (piston or screw driven) or pneumatic forces. DIW is attracting widespread interest in the fields of tissue engineering [2], industrial applications such as batteries [3], sensors [4], four-dimensional (4D) printing [5], soil science [6] and everyday life [7] because it is capable of printing 3D structures in a flexible, low-cost and well-controlled fashion.

The success of DIW process depends on well-printable ink and optimized process parameters. Recent studies [8-10] focused on inks preparation and rheological analyses as ink rheology plays the most critical role in extrusion process, shrinkage, shape fidelity and structural stability. Meanwhile, DIW process parameters concerned with the equipment considerably affect the parts' dimensional accuracy [11].

In 3D printing, dimensional accuracy of printed layers could affect the whole part quality. At present, monitoring and control of printed layers is a research focus in AM quality control [12, 13]. He and Huang [14] predicted the in-plane shape of printed layers to improve the geometric accuracy of AM built products. He et al. [15] captured the image of each printed layer to control the whole process of fused deposition modeling (FDM). Mohammad et al. [16] proposed a quality monitoring framework for 3D printing through monitoring each layer. Therefore, after well-printable inks are prepared to guarantee shape fidelity and structural stability, process parameters optimization for dimensional accuracy of printed layers is necessary for quality control of parts in DIW.

Recently, the selection of process parameters for DIW has been conducted by many scholars [17-19]. However, all these studies just determined a printability window instead of an optimal value and few studies are available for process parameters significance analysis and optimization for DIW. Therefore, it is imperative to investigate the significance of each process parameter and find optimal process parameters setting to improve dimensional accuracy of parts in DIW.

Taguchi method [20] and machine learning (ML) methods [21, 22] have been widely used to control process parameters of material extrusion-based 3D printing. ML methods enable the proper parameters selection with little process analyses but need large dataset, additional time and computing resources [23]. Taguchi technique is more efficient [24] with a significant slash in experimental time and cost [25] and it can determine the significance of each parameter by analysis of variance (ANOVA) [26]. The main purpose of this paper is to perform DIW process parameters optimization with minimum material and time. Thus, Taguchi method is adopted in this study.

In this paper, we identified DIW process parameters through printing analyses and proposed a two-step optimization method to optimize DIW process parameters for dimensional accuracy of printed layers and analyze the significance of each process parameter. To verify the method, confirmation tests were conducted considering the condition comparison and the method robustness on other shapes and other materials; parameter adaptability in 3D parts printing from printed layers' analyses for the proposed method and parameter adaptability in constructs fabricated as 100% infill or with porosities.

2. Materials and methods

2.1. Materials and DIW process

A piston driven DIW 3D printer TM-081 (Tobeca Company, France) was used as illustrated in Figure 1(a). The piston movement is driven by a mechanical system, which extrudes out ink in the syringe through the nozzle into the air and finally on the substrate. Then, a three-axis movement frame guides the nozzle to move in x and y directions to deposit the extruded filaments on a planar region as nozzle is fixed in z direction. Afterward, the nozzle moves to the next layer and 3D parts is printed layer by layer. Finally, the printed part is solidified through heating-based evaporation [27] or ultraviolet (UV) light [28] according to types of printed materials.

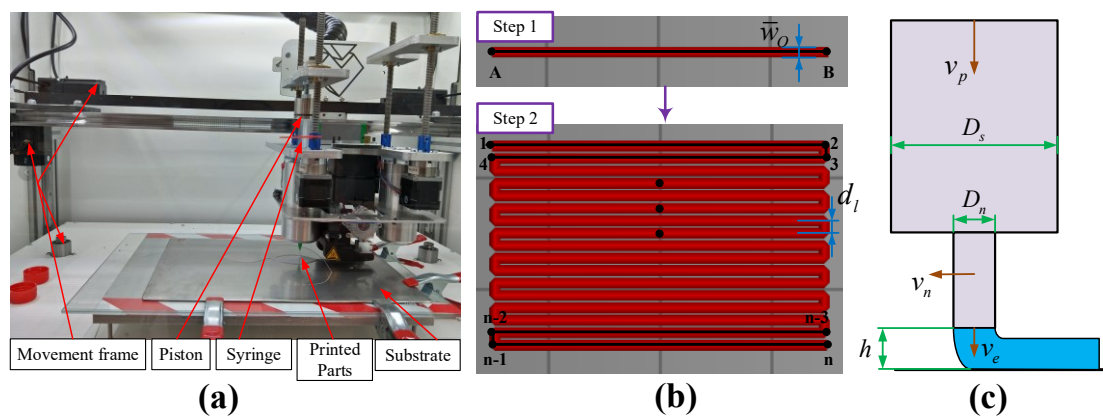


Figure 1. Process parameters identification for DIW process: (a) the DIW 3D printer; (b) the DIW process; (c) process parameters setting in Step 1.

Nivea Crème (Art. No. 80104) (Beiersdorf Global AG, Germany) was chosen as material to verify the proposed method because Nivea Crème is used as printability reference for inks to test the process parameters in DIW and can represent numerous printable inks in DIW [17] (many inks in DIW are designed and produced to have the same printability of Nivea Crème). A complete rheological characterization for Nivea Crème was conducted as ink rheology plays the most critical role in DIW. The yield stress value was determined as 534 Pa through shear stress ramp test (Figure 2(a)), which means the ink stays rest when the shear stress value is below 534 Pa and starts to flow when the shear stress value exceeds 534 Pa. Figure 2(b) shows the shear-thinning characterization of the ink as viscosity decreases with the increase of shear rate. The ink exhibits a solid-like response as its storage modulus (G') exceeds its loss modulus (G'') (Figure 2(c)), which means the ink has low shrinkage and good shape fidelity. Moreover, the structural stability of the ink is also good as shown in Figure 2(d): from 0-200 s, the viscosity stays stable and in high value when shear rate value is near 0; from 200-300 s, the viscosity stays stable and in low value when shear rate value is 900 s^{-1} ; from 300-500 s, the shear rate value recovers to near 0 and the viscosity recovers to stay stable and in high value. In conclusion, Nivea Crème (Art. No. 80104) was verified as a well-printable ink through the rheological characterization. After ink preparation, the focus of this work is to identify and optimize the DIW process parameters.

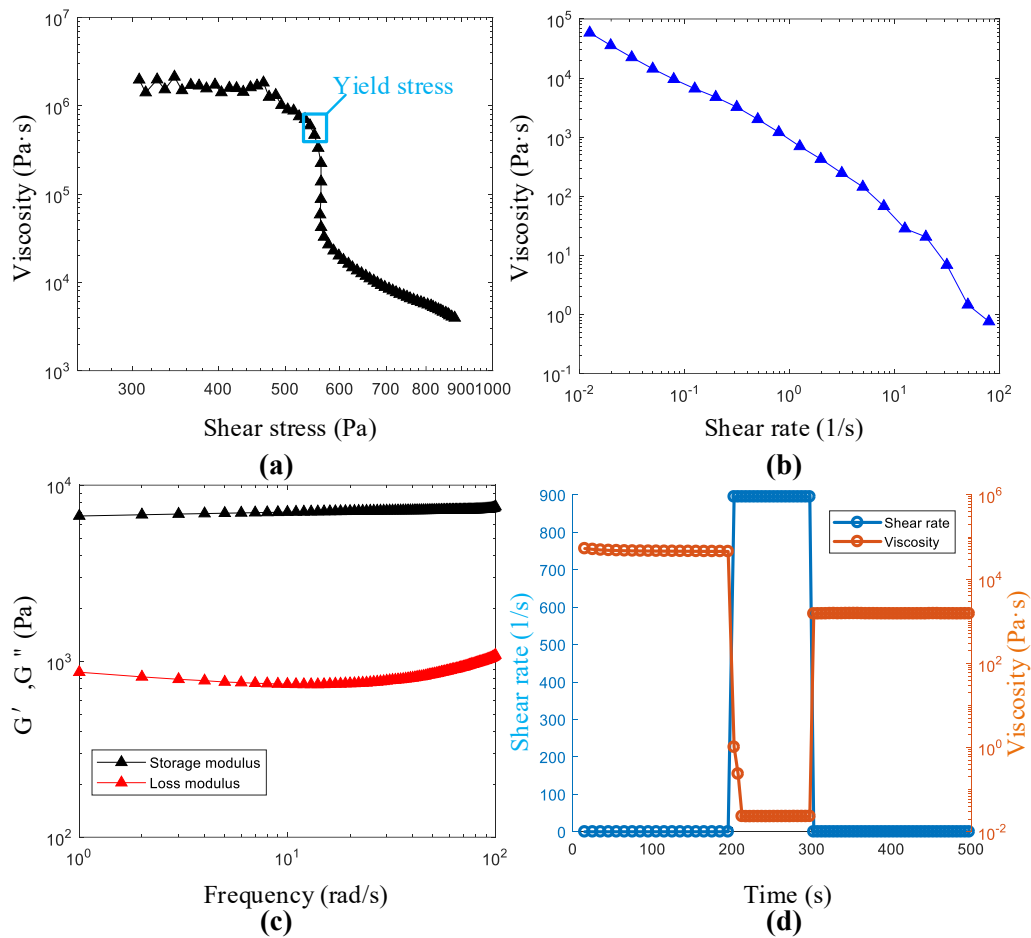


Figure 2. Rheological characterization of Nivea Crème (Art. No. 80104): (a) Yield stress determination through shear stress ramp test; (b) Viscosity as a function of shear rate; (c) Storage (G') and loss (G'') modulus as a function of frequency; (d) stability analysis through recovery test. To verify the method robustness on other materials, a well-printable cellulose-based ink was prepared following the literature [5]. The ingredients of the cellulose-based ink were: 2.36% cellulose fibers, 0.59% hydroxyethylcellulose (HEC), 1.77% carboxymethyl cellulose (CMC), 0.47% montmorillonite, 0.47% citric acid (CA) and 94.34% demineralized water. The detailed preparation process and rheological characterization of the cellulose-based ink can be found in [5].

2.2. Identification of process parameters

Process parameters were identified through DIW process analysis. As shown in Figure 1(b), DIW process for a printed layer includes two steps. Step 1 is to print a line by moving nozzle from point A to point B. Then, a layer is printed by arranging lines tightly in Step 2. Thus, DIW process parameters for printed layers are divided into two categories as:

- 1) Process parameters for printing a line;
- 2) Extra process parameter from lines to a layer.

2.2.1 Process parameters for printing a line

The process parameters for printing a line is illustrated in Figure 1(c). Inner diameters of

syringe tube D_s and nozzle D_n are dependent on equipment and considered as constants. Their values in our study are in 21.6 mm and 0.84 mm respectively. v_p (piston velocity set in the G-code), v_n (nozzle velocity) and h (gap between nozzle bottom surface and substrate) are identified as controllable process parameters. v_e (average velocity of extruded filament on the nozzle bottom surface), which is dependent on v_p and equipment, is uncontrolled process parameters.

In extrusion-based AM, optimal v_n depends on v_p [29] and optimal h depends on D_n [30]. If v_p , v_n and h were set independently without regard to the relationship between these parameters, the optimization would be inefficient and even incorrect. Thus, process parameters for printing a line were identified as: v_n , R_C (calibrated normalization ratio of v_p to v_n) and H (ration of h to D_n , defined as h/D_n).

v_e was used as intermediate variable to define R_C as it is both correlated to v_n and v_p . We supposed that v_n and v_e should satisfy Eq. (1) for optimal process design as follows:

$$v_n = R \cdot v_e. \quad (1)$$

Where R is the ratio of v_n to v_e .

The relationship between real piston velocity and v_e could be calculated according to conservation of mass. However, real piston velocity is not equal to v_p because v_p are nominal values of piston velocity set in the G-code. The main sources of errors between v_p and real piston velocity came from the uncertainty in the control of the piston velocity. To correct systematic errors in the piston velocity control, the relationship between v_p and v_e was calculated using Eq. (2) according to conservation of mass with a calibration procedure [31] as follows:

$$\frac{1}{4} \pi D_s^2 \cdot v_p = C_f \cdot \frac{1}{4} \pi D_n^2 \cdot v_e. \quad (2)$$

Where C_f is a calibration factor which amends the volume conservation to compensate for sources of errors in the piston velocity due to the uncertainty in the control of the piston

velocity.

Eq. (1) and Eq. (2) were combined and simplified into Eq. (3) as follows:

$$v_p = \frac{C_f}{R} \cdot \frac{D_n^2}{D_s^2} \cdot v_n = R_C \cdot \frac{D_n^2}{D_s^2} \cdot v_n. \quad (3)$$

Where R_C is calibrated normalization ratio of v_p to v_n , defined as C_f / R . Identification

of R_C as a process parameter, which considered the relationship between v_p and v_n as well as the main sources of errors in the experiments, improves the efficiency and accuracy of the optimization process.

2.2.2 Extra process parameter from lines to a layer

As illustrated in Figure 1(b), \bar{w}_O (average width of the optimal printed line) of printed line under optimal condition was measured in Step 1. Then, a rectangular object (reprehensive of the printed layers) was printed by controlling d_l (distance between lines) line by line. In extrusion-based AM, optimal d_l depends on \bar{w}_O [32]. Thus, extra process parameter from lines to a layer was identified as R_W (ratio of d_l to \bar{w}_O) and d_l could be determined as follows:

$$d_l = R_W \cdot \bar{w}_O. \quad (4)$$

Where R_W is the ratio of d_l to \bar{w}_O , defined as d_l / \bar{w}_O . R_W mainly reflects the impact of W (the weight of the printed layer) on distortion in x-y plane (detailed relationship between R_W and W as well as its derivation process were shown in the Section SI 1 of Supporting Information (SI)).

Consequently, DIW process parameters were identified as:

- 1) Process parameters for printing a line: v_n , R_C and H ;
- 2) Extra process parameter from lines to a layer: R_W .

2.3. Definition and measurement method of dimensional errors

Dimensional errors were divided into dimensional error for printed lines and dimensional error for printed layers according to the two categories of identified process parameters. x-y plane dimensional accuracy is of primary interest and dimensional accuracy in the z axis can be ignored for layer accuracy analyses because previous studies [12, 14, 16] have verified that the use of control charts with image data only considering x-y plane dimensions for each layer could improve quality of parts in 3D printing significantly.

2.3.1 Dimensional error for printed lines and its measurement method

A. Definition of dimensional error for printed lines

As illustrated in Figure 3(a), N_1 measuring points were set along the line length uniformly and widths of line on each measuring point were measured as $w_i (i = 1, 2, \dots, N_1)$. Average width of the printed line was calculated as follows:

$$\bar{w} = \sum_{i=1}^{N_1} w_i / N_1. \quad (5)$$

Dimensional errors $el_i (i = 1, 2, \dots, N_1)$ on each measuring point along length were defined as follows:

$$el_i = w_i - \bar{w}, (i = 1, 2, \dots, N_1). \quad (6)$$

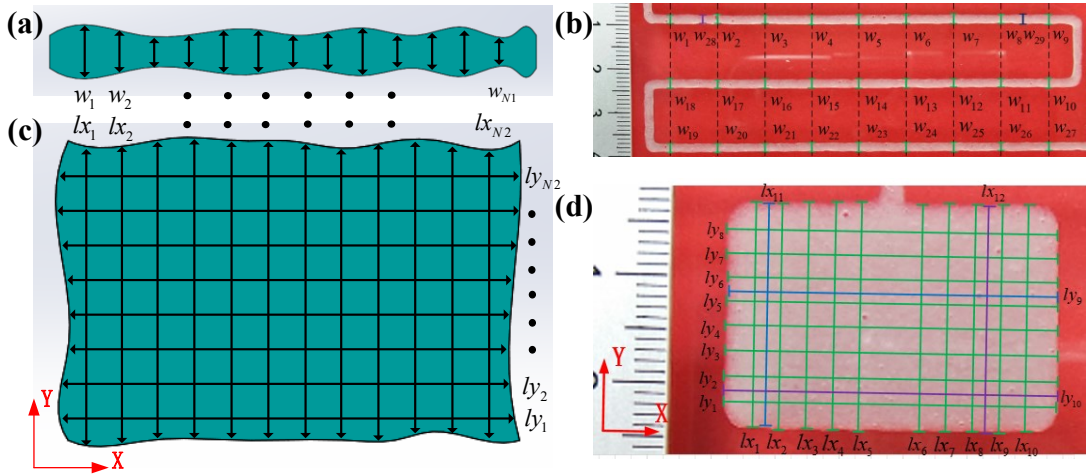


Figure 3. Definition and measurement method of dimensional errors: (a) definition of dimensional errors for printed lines; (b) measuring points setting for printed lines; (c) definition of dimensional errors for printed rectangular objects; (d) measuring points setting for printed rectangular objects.

B. Measurement method of dimensional error for printed lines

As shown in Figure 3(b), to reduce measurement error and consider the printing stability in the whole range, three lines were printed (each line was 100 mm long) and 9 measuring points were set for each line uniformly. 27 measuring points were uniformly distributed along lines as w_1 to w_{27} . Minimum and maximum widths of lines except 27 measuring points was measured as w_{28} and w_{29} . Thus, totally 29 dimensional errors were used for dimensional accuracy analysis of printed lines. In practice, a ruler was put beside printed lines as reference dimension and photo of printed lines with ruler was taken using a camera (Canon LEGRIA HF R86 Noir, Canon Inc., Japan). Then, photo was imported into MATLAB and widths were measured using virtual ruler of the graphic processing tools in MATLAB.

2.3.2 Dimensional error for printed rectangular objects and its measurement method

A. Definition of dimensional error for printed rectangular objects

As illustrated in Figure 3(c), N_2 and N_3 measuring points were set along x and y directions in the printed rectangular object uniformly and lengths on each measuring point along x and y direction were measured as $lx_i (i = 1, 2, \dots, N_2)$ and $ly_i (i = 1, 2, \dots, N_3)$. Average lengths for x and y directions were calculated as follows:

$$\bar{lx} = \sum_{i=1}^{N_2} lx_i / N_2. \quad (7)$$

$$\bar{ly} = \sum_{i=1}^{N_3} ly_i / N_3. \quad (8)$$

Designed dimensions for rectangular object in x and y directions were Lx and Ly . Dimensional errors for the printed rectangular object in x and y directions were defined as follows:

$$erx_i = lx_i - Lx, (i = 1, 2, \dots, N_2). \quad (9)$$

$$ery_i = ly_i - Ly, (i = 1, 2, \dots, N_3). \quad (10)$$

B. Measurement method of dimensional error for printed rectangular objects

To reduce measurement error and consider the printing stability in the whole range, measuring points setting for printed rectangular objects was shown in Figure 3(d). Designed dimensions for rectangular object in x and y directions were $Lx = 30$ mm and $Ly = 20$ mm, respectively. In x direction, 10 measuring points were set uniformly as lx_1 to lx_{10} . Minimum and maximum lengths except 10 points were measured as lx_{11} and lx_{12} . In y direction, 8 measuring points were set uniformly as ly_1 to ly_8 , and minimum and maximum lengths except 8 points were measured as ly_9 and ly_{10} . Thus, 12 lengths were measured in x direction as lx_1 to lx_{12} ; and 10 lengths were measured in y direction as ly_1 to ly_{10} . Totally, 22 dimensional errors were used for dimensional accuracy analysis of printed rectangular objects. In practice, the lengths measurement method was same as widths measurement for printed lines using ruler beside the printed object and MATLAB.

2.4. Orthogonal array selection procedure

Instead of conducting full factorial experiments, Taguchi method based experiments of different process conditions are conducted through an orthogonal array (OA), minimizing the

number of experiments while ensuring the validity and robustness of the data [33]. The OA is selected based on degree of freedom (DOF) calculation considering the number of factors, interactions between them and the number of levels of each factor [34]. The procedure for OA selection is as follows:

- (1) Determine the number, levels and interaction effects of factors.
- (2) Calculate the total DOF of factors. DOF for a single factor is equal to one less than the number of levels of that factor. DOF for a two-factor interaction effect is equal to $(S_1 - 1) \times (S_2 - 1)$ as S_1 and S_2 are DOF of the two factors. Total DOF of factors is cumulative sum of DOF of all single factors and DOF of all two-factor interaction effects.
- (3) OA is selected from commonly used standard OAs based on total DOF of factors as number of experiments should require Eq. (11) as follows [35]:

$$T \geq DOF_{total} + 1. \quad (11)$$

Where T is number of experiments; DOF_{total} is total DOF of factors and their interaction effects.

3. Framework for DIW process optimization

The framework of the two-step process parameters optimization method was shown in Figure 4. Step 1 was to optimize process parameters for printing a line. In step 1, continuity and uniformity of extruded filaments in the air and on the substrate and printed rectangular objects on the substrate were observed in screening experiments to determine printability windows for each process parameter. Then, interaction effect tests were conducted and DOF for experiments was calculated followed by OA selection for Taguchi design. Next, main experiments of line printing based on Taguchi method were conducted. SNR calculations and ANOVA were performed for Taguchi method based data to find the optimal combination and evaluate the significance respectively. Step 2 was to optimize extra process parameter from lines to a layer. In Step 2, the average width of printed lines under optimal condition was obtained firstly. Then, single-factor tests of rectangular object printing were conducted to find the optimal R_{yy} . Finally, the optimal combination of total identified process parameters was summarized through step 1 and step 2 of the framework.

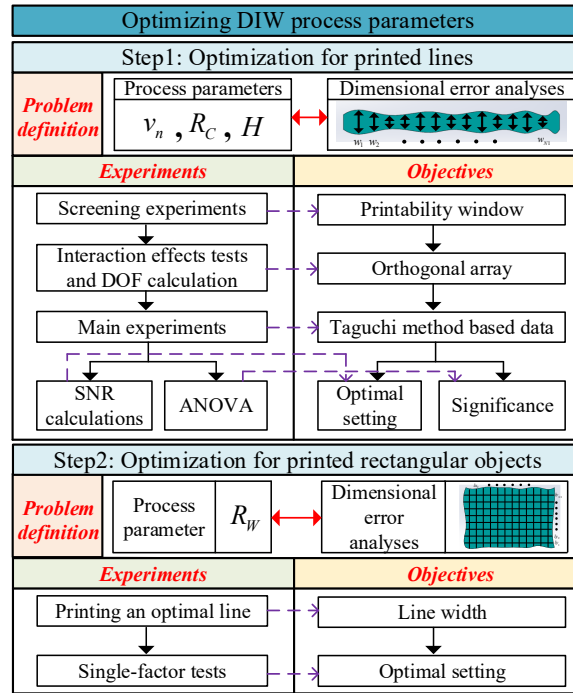


Figure 4. Framework of the proposed two-step method for optimizing DIW process parameters for printed layers.

4. Results and discussion

4.1. Step 1: optimization of printed line

4.1.1 Printability windows

The term ‘printability window’ is defined as the combination of process parameters required for successful extrusion for DIW [17]. In experiments, printability window determination criterions include three points: continuity and uniformity of 1) extruded filaments in the air; 2) extruded filaments on the substrate and 3) printed rectangular object on the substrate.

Detailed information for screening experiments setting were listed in the Section SI 2 of SI. Through screening experiments, printability windows of each process parameter for the prepared ink were listed as: (5~11) mm/s for v_n ; (1~1.6) for R_C ; (0.65~1.05) for H and (0.5~0.9) for R_w .

4.1.2 Orthogonal array selection

The lower value, middle value and higher value of printability windows for each factor in step 1 (v_n , R_C and H) were considered to be level 1, 2 and 3 respectively as listed in Table 1.

Table 1. Levels of process parameters in step 1.

Parameter	Range	Level 1	Level 2	Level 3
v_n	(5~11) mm/s	5	8	11

R_C	1~1.6	1	1.3	1.6
H	0.65~1.05	0.65	0.85	1.05

In this study, only two-factor interaction effects were considered. In interaction effect tests, one factor of v_n , R_C and H was fixed and the remaining two factors were changed to print lines for interaction effect analysis of the remaining two factors. Average widths of printed lines under each process parameters setting were calculated as indicator to analyze interaction effects. Interaction effect graphs were plotted in Figure 5.

Interaction effect graph is a tool to study whether influence of one factor affects the function of the other factors [36]. In the graph, parallel line shows no interaction effect and the intersect or intersect trend between lines means a high degree of interaction [37]. As illustrated in Figure 5, interaction effects of $v_n \times R_C$, $v_n \times H$ and $R_C \times H$ should be considered as two

lines in graphs intersect for $v_n \times R_C$ as well as $v_n \times H$ and had intersect trend for $R_C \times H$.

Thus, three factors (v_n , R_C and H) and three interaction effects ($v_n \times R_C$, $v_n \times H$ and $R_C \times H$) were considered in calculation for total DOF of factors.

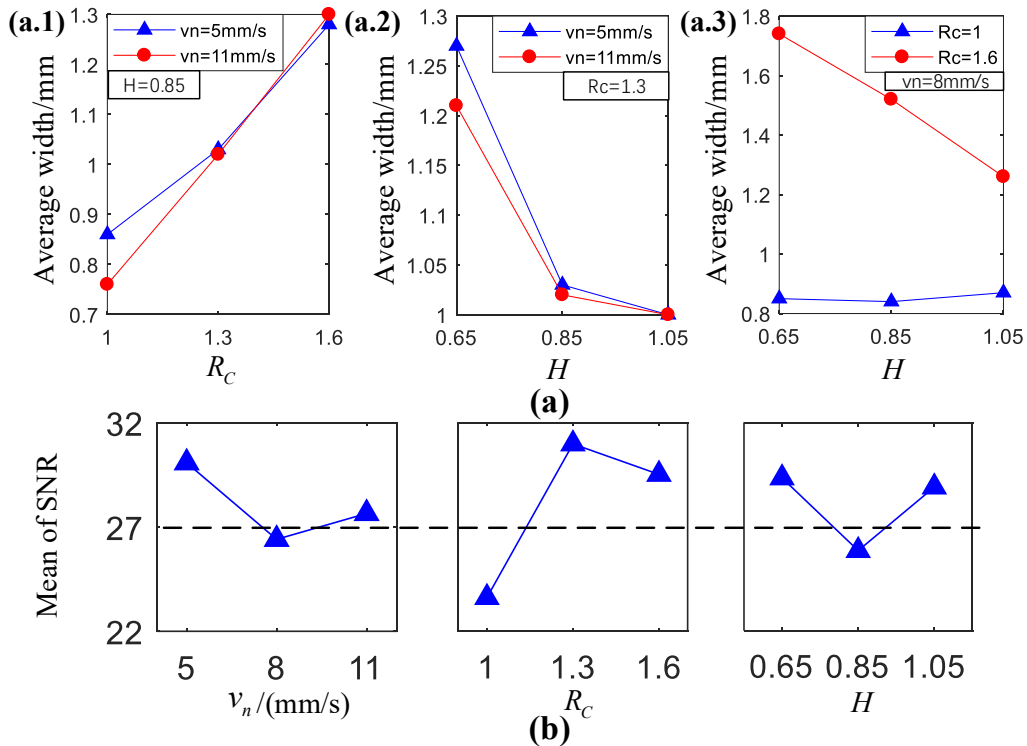


Figure 5. (a) Interaction effect graphs of step1 for: (a.1) $v_n \times R_C$; (a.2) $v_n \times H$; (a.3) $R_C \times H$ and (b) mean SNR graph for main experiments in step 1.

DOF of single factor and their interaction effects were calculated according to Section 2.4 and the total DOF of factors was 18. Thus, L_{27} OA (L_T means OA with T experiments) was

selected for main experiments of step 1 as shown in Table 2, from commonly used standard OAs for three-level Taguchi design including L_9 , L_{18} and L_{27} according to Eq. (11).

Table 2. Experimental plan and calculated SNR for main experiments of step 1.

Experiment number	Experimental condition			SNR of dimensional errors
	v_n / (mm/s)	R_c	H	
N1	5	1	0.65	22.51
N2	5	1	0.85	18.75
N3	5	1	1.05	22.73
N4	5	1.3	0.65	31.60
N5	5	1.3	0.85	28.22
N6	5	1.3	1.05	42.12
N7	5	1.6	0.65	38.58
N8	5	1.6	0.85	30.33
N9	5	1.6	1.05	35.91
N10	8	1	0.65	20.81
N11	8	1	0.85	20.64
N12	8	1	1.05	22.07
N13	8	1.3	0.65	37.32
N14	8	1.3	0.85	33.76
N15	8	1.3	1.05	25.78
N16	8	1.6	0.65	22.82
N17	8	1.6	0.85	25.37
N18	8	1.6	1.05	29.11
N19	11	1	0.65	36.61
N20	11	1	0.85	24.71
N21	11	1	1.05	23.74
N22	11	1.3	0.65	27.22
N23	11	1.3	0.85	26.96
N24	11	1.3	1.05	25.94
N25	11	1.6	0.65	26.78
N26	11	1.6	0.85	23.98
N27	11	1.6	1.05	32.92

4.1.3 SNR analysis

Main experiments of step 1, containing 27 experimental runs, were conducted as shown in Table 2. Based on the requirements of response, SNR was divided into three categories namely medium-the-better, higher-the-better and lower-the-better [38]. In this study, the dimensional error is the lower-the-better to enhance the printing accuracy. Hence, Eq. (12) was used to calculate the SNR; and results were listed in Table 2.

$$\eta = -10 \log \left(\frac{1}{n} \sum_{i=1}^n y_i^2 \right). \quad (12)$$

Where η was the average SNR, n was the number of experiments conducted at level i and y_i was the evaluation value (dimensional error in this study).

The mean SNR response of each process parameters in each level was calculated and listed in Table 3. Figure 5(b) represented the mean SNR graph. Higher SNR represents the minimum variation difference between the desired output and evaluated output. Therefore, optimal process parameters for high dimensional accuracy using Taguchi method were found as: $v_n = 5$ mm/s, $R_C = 1.3$, $H = 0.65$.

Table 3. Mean SNR response table for dimensional error of main experiments in step 1.

Process parameters	Mean SNR for dimensional error			Max-Min	Rank
	Level 1	Level 2	Level 3		
v_n	30.08	27.65	27.65	3.67	2
R_C	23.62	29.53	29.53	7.37	1
H	29.36	28.92	28.92	3.50	3

4.1.4 ANOVA results

ANOVA is a tool to investigate the significant effect and indicate the contribution of process parameters in machinability researches [39]. ANOVA results for dimensional error of printed lines obtained using Minitab software was shown in Table 4. From Table 4, it was found that dimensional error was significantly influenced by R_C followed by $v_n \times R_C$, $v_n \times H$, H , v_n and $R_C \times H$. The contribution percentage of process parameters setting for R_C , H and v_n on dimensional error was 27.78%, 6.64% and 6.37%, respectively, meaning R_C is the most important process parameters for dimensional error of printed lines. Meanwhile, interaction effects of $v_n \times R_C$, $v_n \times H$ and $R_C \times H$ influenced dimensional error in 26.65%, 7.01% and 4.41% percentage of contribution respectively. Thus, OA selection for Taguchi design should consider interaction effects of $v_n \times R_C$, $v_n \times H$ and $R_C \times H$ as interaction effects of $v_n \times R_C$, $v_n \times H$ and $R_C \times H$ had big influences on dimensional error. R_C is highly significant in dimensional error at 95% level of confidence as p-value < 0.05. Thus, R_C was principal in single process parameters setting which should be paid more attention in DIW.

Table 4. ANOVA of dimensional error for main experiments in step 1.

Source	DOF	Sum of squares (SS)	Mean squares (MS)	F-ratio	p value	Contribution (%)
--------	-----	---------------------	-------------------	---------	---------	------------------

v_n	2	62.90	31.45	1.21	0.349	6.37
R_C	2	274.31	137.15	5.26	0.035	27.78
H	2	65.58	32.79	1.26	0.335	6.64
$v_n \times R_C$	4	263.16	65.79	2.52	0.124	26.65
$v_n \times H$	4	69.26	17.31	0.66	0.635	7.01
$R_C \times H$	4	43.52	10.88	0.42	0.792	4.41
Error	8	208.77	26.10			21.14
Total	26	987.50				100

4.2. Step 2: optimization of printed rectangular objects

4.2.1 Line width under optimal process parameters

At the beginning of step 2, lines were printed using optimal process parameters obtained in step 1 to get line width under optimum condition. Average width of the optimal printed line was calculated using Eq. (5) as 1.31 mm.

4.2.2 Single-factor tests

In order to get a layer from lines, distance between lines d_l was calculated by Eq. (4). In Eq. (4), average width of optimal lines \bar{w}_O was obtained at the beginning of step 2; and only single-factor R_W determines printing results in step 2. Single-factor tests, containing 5 experimental runs, were conducted as shown in Table 5 to find optimal value of R_W . The lower-the-better SNR was used and results were listed in Table 5. Higher SNR represents better dimensional accuracy. Therefore, optimal R_W were found as: $R_W = 0.9$.

Table 5. Single-factor tests for step 2.

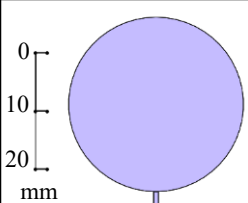
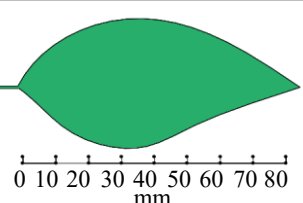

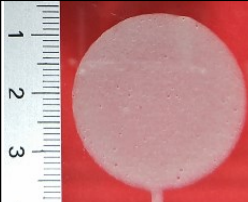


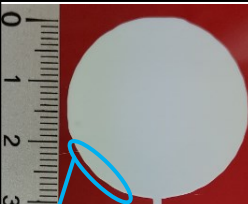
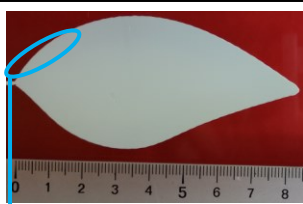
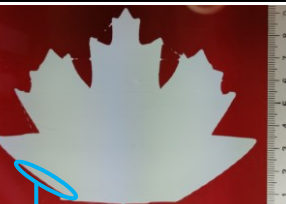
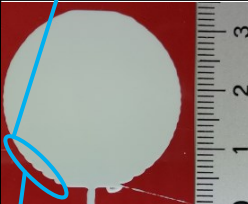
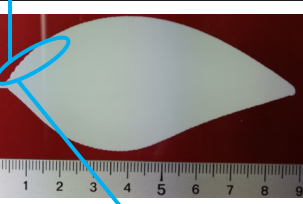

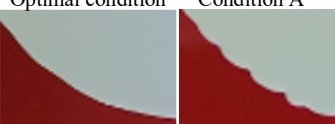
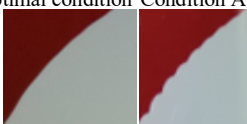

Experiment number	NR1	NR2	NR3	NR4	NR5
R_W	0.5	0.6	0.7	0.8	0.9
SNR of dimensional error	1.96	0.88	1.73	0.38	16.95

Consequently, optimal DIW process parameters for a layer fabricated in the prepared ink were found as: $v_n = 5$ mm/s, $R_C = 1.3$, $H = 0.65$, $R_W = 0.9$.

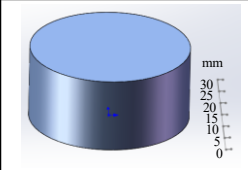
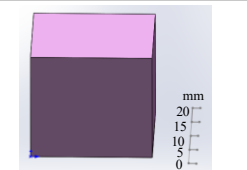
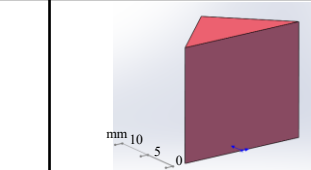



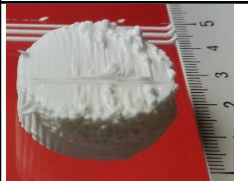
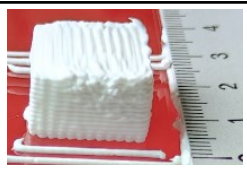

4.3. Confirmation tests

4.3.1 Confirmation tests for method robustness on shapes

To validate that the optimum conditions can be generalized to layers in other shapes, three shapes as Shape A (disk), Shape 2 (leaf) and Shape C (maple leaf) were printed under optimal condition (**achieved by proposed method**) and condition A ($v_n = 8$ mm/s, $R_C = 1$, $H = 0.85$, $R_W = 0.8$). As shown in Figure 6(a), the dimensional quality under optimal condition was higher than that under condition A, verifying the method robustness in other shapes.

Item	Condition	(Shape A)	(Shape B)	(Shape C)
Designed shape				
Printed single layers	Cellulose-based ink under optimal condition			
	Nivea Crème under optimal condition			
	Nivea Crème under condition A			
		Optimal condition Condition A	Optimal condition Condition A	Optimal condition Condition A
				

(a)

Item	Material	(Model A)	(Model B)	(Model C)
Designed model				
Printed 3D parts	Nivea Crème under optimal condition			
	Nivea Crème under condition A			

(b)

Figure 6. Confirmation tests for the proposed method in (a) verification of method robustness on layer shapes and materials; (b) verification for parameter adaptability in 3D parts printing.

4.3.2 Confirmation tests for method robustness on materials

To verify the method robustness on materials, a well-printable cellulose-based ink was chosen. The optimized process parameters for the cellulose-based ink in DIW obtained using the proposed method were: $v_n = 10$ mm/s, $R_C = 1.5$, $H = 0.25$, $R_W = 0.5$. As shown in Figure 6(a), printed layers in three shapes using the cellulose-based ink have high dimensional accuracy same as Nivea Crème, verifying the method robustness on materials. Moreover, compared with the optimized process parameters for cellulose-based ink (low viscosity) and Nivea Crème (high viscosity), it could be concluded that ink with higher viscosity in DIW needs smaller values for v_n , R_C and larger values for H , R_W .

4.3.3 Confirmation tests for parameter adaptability in 3D parts printing

In order to verify the adaptability of optimized process parameter from printed layers' analyses in 3D parts printing, three 3D models were printed using the same optimized process parameters and layer height was set as h for printed layers in Nivea Crème based DIW. As shown in Figure 6(b), the printed 3D parts had good dimensional quality by comparing printed parts under optimal condition and condition A ($v_n = 8$ mm/s, $R_C = 1$, $H = 0.85$, $R_W = 0.8$), verifying that the proposed method has parameter adaptability in 3D parts printing from printed layers.

4.3.4 Confirmation tests for parameter adaptability in constructs with porosities

To verify the adaptability of optimized process parameter for constructs with porosities, confirmation tests were conducted as shown in Figure 7. Two grids named as Grids A and Grids B were designed as shown in Figure 7(a): the total dimensions of grids A and grids B are same in 31.2 mm X 31.2 mm; and the dimensions of porosity in grids A and grids B are 3 mm X 3 mm and 6.8 mm X 6.8 mm, respectively. As shown in Figure 7(b) and Figure 7(c), the printed single-layer and 10-layers grids had good dimensional quality by comparing printed grids under optimal condition and condition A ($v_n = 8$ mm/s, $R_C = 1$, $H = 0.85$, $R_W = 0.8$), verifying that the proposed method has parameter adaptability in constructs with porosities.

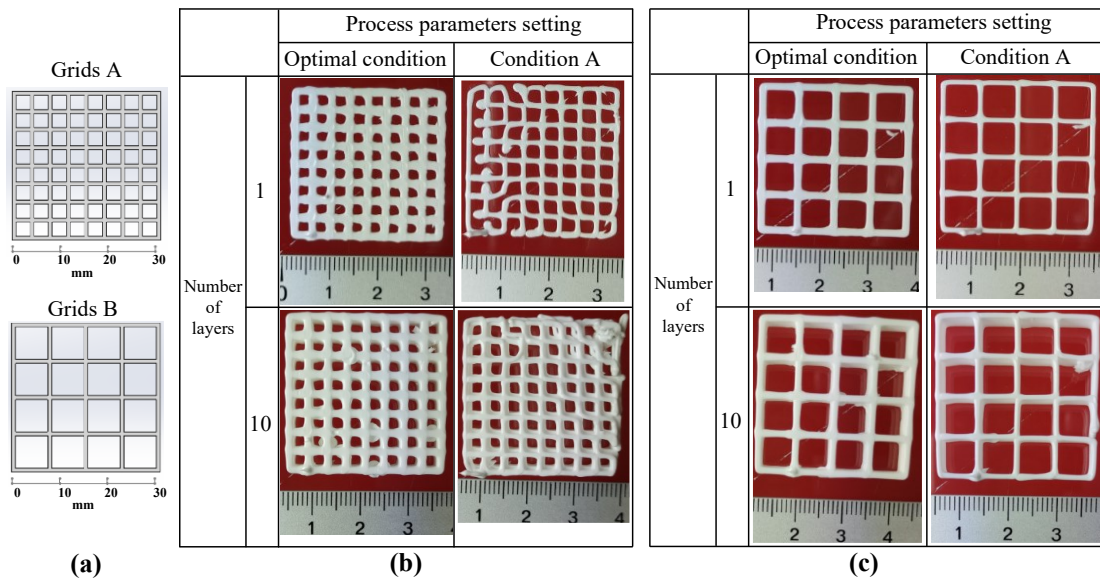


Figure 7. Confirmation tests for the proposed method in constructs with porosities: (a) two designed grids: grids A and grids B; (b) printed grids A under optimal condition and condition A in single layer and 10-layers; (c) printed grids B under optimal condition and condition A in single layer and 10-layers.

4.4. Contributions and future work

Dimensional accuracy of printed parts in DIW depends both on inks' material properties (especially rheological properties) and process parameters. To fully understand DIW, mathematical and simulation models were established to predict printing resolution using rheological properties and process parameters as input factors [40-42]. However, scholars were focusing on inks preparation and rheological analyses to realize a successful DIW and process parameters were determined by simple variable tests. Few work fully analyzed process parameters. It is useful and necessary to analyze process parameters through process analyses and optimize them as process parameters identification and optimization are important for DIW applications. This work focuses on the identification and optimization of process parameters for well-printable inks (such as Nivea Crème and cellulose-based ink) whose rheological properties are already analyzed in the literature. The contributions of this work include: (a) key process parameters identification through process analyses; (b) process parameters optimization through the proposed two-step method.

In the future, a model for DIW using the identified process parameters in this work and inks' rheological properties as input factors through analytical and simulation methods will be established to fully understand the DIW process.

5. Conclusion

In this study, the DIW process parameters were identified through process analyses and a two-step method was proposed to optimize DIW process parameters for dimensional accuracy and analyze the significance of each process parameter.

In the DIW process parameters identification, DIW process parameters for printed layers were divided into two categories and identified by process analysis as: 1) process parameters for printing a line and 2) extra process parameter from lines to a layer. The process parameters

identification considered the relationship between intermediate process parameters as well as main sources of errors in the experiments, thus improved the efficiency and accuracy of the optimization process. In the two-step optimization method for identified DIW process parameters, Step 1 was to optimize process parameters for printing a line and Step 2 was to optimize the parameter from lines to a layer. Confirmation results verified the proposed method and the method robustness on other shapes and other materials; parameter adaptability in 3D parts printing from printed layers' analyses for the proposed method and parameter adaptability in constructs fabricated as 100% infill or with porosities. This proposed two-step optimization method satisfies the requirement of high quality DIW process by finding optimum process parameters setting with minimum materials and time. The proposed method will allow a rapid and reproducible process parameters optimization of a wide variety of inks in DIW.

Author Disclosure Statement

No competing financial interests exist.

Funding Information

The authors would like to acknowledge the funding from the China Scholarship Council scholarship (No. 201906020135).

References

- [1] S. Tarassoli, Z. Jessop, A. Al-Sabah, I. Simoes, and I. Whitaker, "Searching for the optimal bioink in extrusion-based 3D bioprinting for reconstructive surgery," *International Journal of Surgery*, vol. 55, p. S95, 2018/07/01/ 2018.
- [2] D. F. D. Campos *et al.*, "Synchronized Dual Bioprinting of Bioinks and Biomaterial Inks as a Translational Strategy for Cartilage Tissue Engineering," *3D Printing and Additive Manufacturing*, vol. 6, no. 2, pp. 63-71, 2019/04/01 2019.
- [3] D. Cao *et al.*, "3D Printed High-Performance Lithium Metal Microbatteries Enabled by Nanocellulose," *Advanced Materials*, vol. 31, no. 14, p. 1807313, 2019/04/01 2019.
- [4] T. Kim, C. Bao, M. Hausmann, G. Siqueira, T. Zimmermann, and W. S. Kim, "3D Printed Disposable Wireless Ion Sensors with Biocompatible Cellulose Composites," *Advanced Electronic Materials*, vol. 5, no. 2, p. 1800778, 2019/02/01 2019.
- [5] M. C. Mulakkal, R. S. Trask, V. P. Ting, and A. M. Seddon, "Responsive cellulose-hydrogel composite ink for 4D printing," *Materials & Design*, vol. 160, pp. 108-118, 2018/12/15/ 2018.
- [6] J. A. Arrieta-Escobar *et al.*, "3D printing: An emerging opportunity for soil science," *Geoderma*, vol. 378, p. 114588, 2020/11/15/ 2020.
- [7] J. S. Park, T. Kim, and W. S. Kim, "Conductive Cellulose Composites with Low Percolation Threshold for 3D Printed Electronics," *Scientific Reports*, vol. 7, no. 1, p. 3246, 2017/06/12 2017.
- [8] G. Siqueira *et al.*, "Cellulose Nanocrystal Inks for 3D Printing of Textured Cellular Architectures," *Advanced Functional Materials*, <https://doi.org/10.1002/adfm.201604619>

vol. 27, no. 12, p. 1604619, 2017/03/01 2017.

- [9] L. del-Mazo-Barbara and M.-P. Ginebra, "Rheological characterisation of ceramic inks for 3D direct ink writing: a review," *Journal of the European Ceramic Society*, 2021/08/18/ 2021.
- [10] B. Román-Manso, J. Muth, L. J. Gibson, W. Ruettinger, and J. A. Lewis, "Hierarchically Porous Ceramics via Direct Writing of Binary Colloidal Gel Foams," *ACS Applied Materials & Interfaces*, vol. 13, no. 7, pp. 8976-8984, 2021/02/24 2021.
- [11] B. Luo, H. Chen, Z. Zhu, B. Xie, C. Bian, and Y. Wang, "Printing single-walled carbon nanotube/Nafion composites by direct writing techniques," *Materials & Design*, vol. 155, pp. 125-133, 2018/10/05/ 2018.
- [12] Z. Jin, Z. Zhang, and G. X. Gu, "Autonomous in-situ correction of fused deposition modeling printers using computer vision and deep learning," *Manufacturing Letters*, vol. 22, pp. 11-15, 2019/10/01/ 2019.
- [13] A. L. Petsiuk and J. M. Pearce, "Open source computer vision-based layer-wise 3D printing analysis," *Additive Manufacturing*, vol. 36, p. 101473, 2020/12/01/ 2020.
- [14] H. Luan and Q. Huang, "Prescriptive Modeling and Compensation of In-Plane Shape Deformation for 3-D Printed Freeform Products," *IEEE Transactions on Automation Science and Engineering*, vol. 14, no. 1, pp. 73-82, 2017.
- [15] K. He, Q. Zhang, and Y. Hong, "Profile monitoring based quality control method for fused deposition modeling process," *J. Intell. Manuf.*, vol. 30, no. 2, pp. 947-958, 2019.
- [16] M. Najjartabar Bisheh, S. I. Chang, and S. Lei, "A layer-by-layer quality monitoring framework for 3D printing," *Computers & Industrial Engineering*, vol. 157, p. 107314, 2021/07/01/ 2021.
- [17] N. Paxton, W. Smolan, T. Böck, F. Melchels, J. Groll, and T. Jungst, "Proposal to assess printability of bioinks for extrusion-based bioprinting and evaluation of rheological properties governing bioprintability," *Biofabrication*, vol. 9, no. 4, p. 044107, 2017/11/14 2017.
- [18] M. H. Kim, Y. W. Lee, W.-K. Jung, J. Oh, and S. Y. Nam, "Enhanced rheological behaviors of alginate hydrogels with carrageenan for extrusion-based bioprinting," *Journal of the Mechanical Behavior of Biomedical Materials*, vol. 98, pp. 187-194, 2019/10/01/ 2019.
- [19] F. Koch, K. Tröndle, G. Finkenzeller, R. Zengerle, S. Zimmermann, and P. Koltay, "Generic method of printing window adjustment for extrusion-based 3D-bioprinting to maintain high viability of mesenchymal stem cells in an alginate-gelatin hydrogel," *Bioprinting*, vol. 20, p. e00094, 2020/12/01/ 2020.
- [20] G. Dong, G. Wijaya, Y. Tang, and Y. F. Zhao, "Optimizing process parameters of fused deposition modeling by Taguchi method for the fabrication of lattice structures," *Additive Manufacturing*, vol. 19, pp. 62-72, 2018/01/01/ 2018.
- [21] P. Meißner, H. Watschke, J. Winter, and T. Vietor, "Artificial Neural Networks-Based Material Parameter Identification for Numerical Simulations of Additively Manufactured Parts by Material Extrusion," *Polymers*, vol. 12, no. 12, 2020.
- [22] L. Li, R. McGuan, R. Isaac, P. Kavehpour, and R. Candler, "Improving precision of material extrusion 3D printing by in-situ monitoring & predicting 3D geometric deviation using conditional adversarial networks," *Additive Manufacturing*, vol. 38, p. 101695, 2021/02/01/ 2021.

- [23] G. D. Goh, S. L. Sing, and W. Y. Yeong, "A review on machine learning in 3D printing: applications, potential, and challenges," *Artificial Intelligence Review*, vol. 54, no. 1, pp. 63-94, 2021/01/01 2021.
- [24] G. Papazetis and G.-C. Vosniakos, "Mapping of deposition-stable and defect-free additive manufacturing via material extrusion from minimal experiments," *The International Journal of Advanced Manufacturing Technology*, vol. 100, no. 9, pp. 2207-2219, 2019/02/01 2019.
- [25] S. Mahmood, A. J. Qureshi, and D. Talamona, "Taguchi based process optimization for dimension and tolerance control for fused deposition modelling," *Additive Manufacturing*, vol. 21, pp. 183-190, 2018/05/01/ 2018.
- [26] U. K. u. Zaman, E. Boesch, A. Siadat, M. Rivette, and A. A. Baqai, "Impact of fused deposition modeling (FDM) process parameters on strength of built parts using Taguchi's design of experiments," *The International Journal of Advanced Manufacturing Technology*, vol. 101, no. 5, pp. 1215-1226, 2019/04/01 2019.
- [27] M. Kim and J.-W. Choi, "Rubber ink formulations with high solid content for direct-ink write process," *Additive Manufacturing*, vol. 44, p. 102023, 2021/08/01/ 2021.
- [28] C. B. Arrington, D. A. Rau, C. B. Williams, and T. E. Long, "UV-assisted direct ink write printing of fully aromatic Poly(amide imide)s: Elucidating the influence of an acrylic scaffold," *Polymer*, vol. 212, p. 123306, 2021/01/06/ 2021.
- [29] R. Comminal, M. P. Serdeczny, D. B. Pedersen, and J. Spangenberg, "Motion planning and numerical simulation of material deposition at corners in extrusion additive manufacturing," *Additive Manufacturing*, vol. 29, p. 100753, 2019/10/01/ 2019.
- [30] R. Comminal, M. P. Serdeczny, D. B. Pedersen, and J. Spangenberg, "Numerical modeling of the strand deposition flow in extrusion-based additive manufacturing," *Additive Manufacturing*, vol. 20, pp. 68-76, 2018/03/01/ 2018.
- [31] M. P. Serdeczny, R. Comminal, D. B. Pedersen, and J. Spangenberg, "Experimental validation of a numerical model for the strand shape in material extrusion additive manufacturing," *Additive Manufacturing*, vol. 24, pp. 145-153, 2018/12/01/ 2018.
- [32] M. P. Serdeczny, R. Comminal, D. B. Pedersen, and J. Spangenberg, "Numerical simulations of the mesostructure formation in material extrusion additive manufacturing," *Additive Manufacturing*, vol. 28, pp. 419-429, 2019/08/01/ 2019.
- [33] F. Guo, X. Zhou, J. Liu, Y. Zhang, D. Li, and H. Zhou, "A reinforcement learning decision model for online process parameters optimization from offline data in injection molding," *Applied Soft Computing*, vol. 85, p. 105828, 2019/12/01/ 2019.
- [34] K. Chockalingam, N. Jawahar, K. N. Ramanathan, and P. S. Banerjee, "Optimization of stereolithography process parameters for part strength using design of experiments," *The International Journal of Advanced Manufacturing Technology*, vol. 29, no. 1, pp. 79-88, 2006/05/01 2006.
- [35] H. X. Li, Y. Li, B. Jiang, L. Zhang, X. Wu, and J. Lin, "Energy performance optimisation of building envelope retrofit through integrated orthogonal arrays with data envelopment analysis," *Renewable Energy*, vol. 149, pp. 1414-1423, 2020/04/01/ 2020.
- [36] G. Senthilkumar and R. Ramakrishnan, "A study of individual and interaction effect of process parameters on friction welded AISI 410 and AISI 430 joint," *Materials Today: Proceedings*, 2020/12/26/ 2020.

- [37] N.-H. Kim, M.-H. Choi, S.-Y. Kim, and E.-G. Chang, "Design of experiment (DOE) method considering interaction effect of process parameters for optimization of copper chemical mechanical polishing (CMP) process," *Microelectronic Engineering*, vol. 83, no. 3, pp. 506-512, 2006/03/01/ 2006.
- [38] P. Sivaiah and D. Chakradhar, "Modeling and optimization of sustainable manufacturing process in machining of 17-4 PH stainless steel," *Measurement*, vol. 134, pp. 142-152, 2019/02/01/ 2019.
- [39] P. Geng *et al.*, "Effects of Printing Parameters on the Mechanical Properties of High-Performance Polyphenylene Sulfide Three-Dimensional Printing," *3D Printing and Additive Manufacturing*, vol. 8, no. 1, pp. 33-41, 2021/02/01 2020.
- [40] R. Suntornnond, E. Y. Tan, J. An, and C. K. Chua, "A Mathematical Model on the Resolution of Extrusion Bioprinting for the Development of New Bioinks," *Materials*, vol. 9, no. 9, 2016.
- [41] A. La Gala, R. Fiorio, M. Erkoç, L. Cardon, and D. R. D'hooge, "Theoretical Evaluation of the Melting Efficiency for the Single-Screw Micro-Extrusion Process: The Case of 3D Printing of ABS," *Processes*, vol. 8, no. 11, 2020.
- [42] Q. Liu *et al.*, "Assessing the dynamic extrusion-based 3D printing process for power-law fluid using numerical simulation," *Journal of Food Engineering*, vol. 275, p. 109861, 2020/06/01/ 2020.